IEEE Access
Multidisciplinary | Rapid Review | Open Access Journal

Received 27 June 2022, accepted 19 July 2022, date of publication 25 July 2022, date of current version 29 July 2022.

Digital Object Identifier 10.1109/ACCESS.2022.3193491

RESEARCH ARTICLE

Distributed Islanding Detection in Multisource DC Microgrids: Pilot Signal Cancelation

CRISTIAN BLANCO[1], (Member, IEEE), FRANCISCO PAZ[2], (Member, IEEE), IGNACIO GALIANO ZURBRIGGEN[3], (Member, IEEE), PABLO GARCIA[1], (Senior Member, IEEE), AND MARTIN ORDONEZ[2], (Member, IEEE)

[1]LEMUR Research Group, University of Oviedo, 33204 Gijon, Spain
[2]Department of Electrical and Computer Engineering, The University of British Columbia, Vancouver, BC V6T 1Z4, Canada
[3]Department of Electrical and Software Engineering, University of Calgary, Calgary, AB T2N 1N4, Canada

Corresponding author: Cristian Blanco (blancocristian@uniovi.es)

This work was supported in part by the Spanish Ministry of Science, Innovation and Universities under the 2019 Jose Castillejo under Grant CAS19-329; in part by the European Union's H2020 Research and Innovation Program under Grant 864459 (UE-19-TALENT-864459); and in part by the Ministry of Science, Innovation and Universities through MCIN/AEI/10.13039/501100011033 under Grant MCI-20-PID2019-111051RB-I00.

ABSTRACT Integrating Distributed Generators (DGs) in DC microgrids require islanding detection in all converters. Impedance-based islanding detection methods can be beneficial in single-converter scenarios. However, their implementation in multi-converter systems is challenging due to interference among DGs. This paper proposes a Leader/Follower strategy for each active participant of the DC microgrid to independently detect the grid connection state. While the Leader injects a small AC pilot signal to estimate the impedance at its terminals, the Followers implement the proposed pilot signal cancellation (PSC) to present a virtual disconnection from the bus at ω_p. This leads to two core benefits: the Leader does not receive interference from the input impedance of the followers yielding accurate islanding detection for the Leader, and the followers can detect the islanding condition independently, with no need to increase the PSC amplitude. The proposed method provides independent and simultaneous islanding detection for all active participants in the DC microgrid. At the same time, it is scalable by the number of parallel-converters, not requiring any communication. Finally, the method has a minimal effect on the bus voltage.

INDEX TERMS Current control, DC microgrids, DC-DC power converters, hybrid power systems, impedance measurement, islanding, microgrids, noise cancellation.

NOMENCLATURE

AC	Alternating Current.
B	Breaker connecting the grid forming converter to the PCC.
BPF	Band-Pass Filter.
$BPF(s)$	Transfer function of the BPF.
BW	Bandwith of a controller or filter.
C_l	Output capacitor of the Leader converter.
C_{fx}	Output capacitor of the x-th follower converter.
CPL	Constant Power Load.
DC	Direct current.
DG	Distributed Generator.
EV	Electric Vehicle.
i_g	Output current of the AC/DC converter interfacing the grid.
$i^*_{L_{pl}}$	Pilot signal reference current to the current loop of the Leader converter.
$i^*_{L_{DC_l}}$	DC reference current to the current loop of the Leader converter.
i_{Ll}	Inductor current of the Leader converter.
i_{Lfx}	Inductor current of the x-th follower converter.
i_{ol}	Output current of the Leader converter.
i_{ofx}	Output current of the x-th Follower converter.
L_g	Equivalent series inductance on the DC side of the AC/DC converter that interfaces the AC grid.

The associate editor coordinating the review of this manuscript and approving it for publication was Zhilei Yao.

L_l	Inductance of the Leader converter.
L_{fx}	Inductance of the x-th Follower converter.
PCC	Point of Common Coupling.
PI	Proportional Integral [controller].
PR	Proportional Resonant [controller].
PSC	Pilot Signal Cancellation.
PV	Photovoltaic.
QSG	Quadrature Signal Generator.
R	Equivalent resistance of all the loads connected to the DC microgrid.
R_g	Equivalent series resistance on the DC side of the AC/DC converter that interfaces the AC grid.
ROCOV	Rate of Change of Voltage islanding detection method.
SVS	Sandia Voltage Shift islanding detection method.
SOGI	Second order generalized integrator.
v_{cmdfx}	Command voltage of the PSC method in the x-th Follower converter.
v_{ol}	Output voltage of the Leader converter.
v_{ofx}	Output voltage of the x-th Follower converter.
ω_p	Angular frequency of the injected AC pilot signal.
Z_{ll}	Impedance of the line connecting the Leader converter to the PCC.
Z_{lfx}	Impedance of the line connecting the x-th follower converter to the PCC.
$\vec{\hat{Z}}_o$	Output impedance estimation of from the leader converter at ω_p.

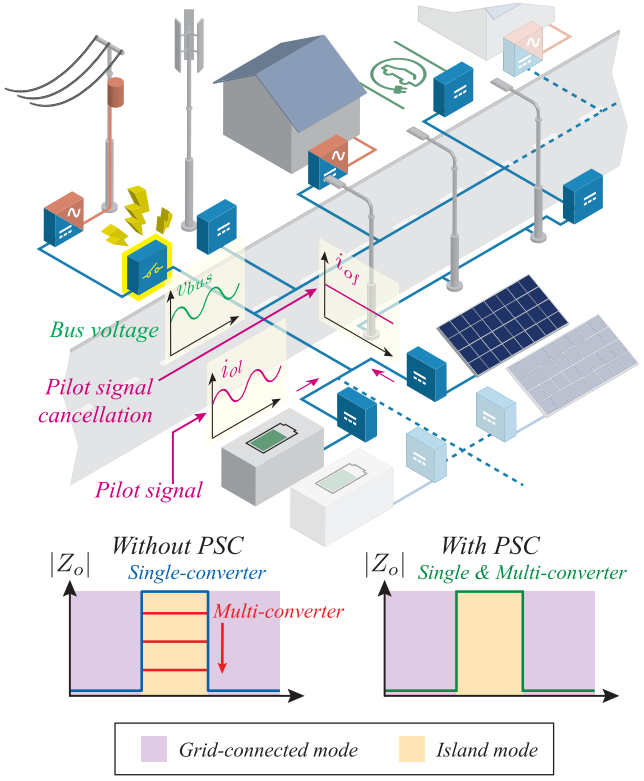

FIGURE 1. Hybrid AC/DC microgrid showing the islanding detection dilemma in a multi-converter scenario and the proposed technique applied to impedance detection. PSC stands for Pilot Signal Cancellation (PSC). It can be observed that in the case of implementing an impedance estimation method based on the injection of an AC signal, the difference between grid-connected and island decreases with the connection of extra converters in parallel. The proposed method completely solves this problem, and also provides simultaneous detection in all converters of the microgrid.

I. INTRODUCTION

In the previous decades, microgrids have been the focus of major efforts to develop low-carbon footprint technologies. Microgrids usually include distributed generators (DGs), energy storage systems, heating, lighting, and more recently, electric vehicles. Although the AC microgrids were first studied, in the past ten years, DC and AC/DC hybrid microgrids have grown in popularity since renewable generation, some loads, and storage technologies are naturally in DC, [1], [2]. At the same time, working in DC shows some advantages like improved efficiency or reduction of power conversion stages.

Figure 1 shows a hybrid AC/DC microgrid structure. Generation units (PV modules) are connected to a common DC bus with energy storage systems, street lighting, EV charging stations, telecommunication systems, and a few inverters for home or industrial supplies. The DC side of the microgrid interfaces the main AC grid through a bidirectional AC/DC converter. DC/DC converters are used to connect energy storage systems, PV systems or other types of loads and generators. They come in a variety of topologies in practice [3]–[8]. Although control strategies are generally simpler in DC than in AC [9], in such a complex scenario, control and protection strategies play an important role [10]. The use of different DGs (PV, micro-wind, fuel cell…), loads, and energy storage systems within the common DC bus create difficulties in the management of DC bus voltage due to power-sharing [11]; AC/DC converters are usually in charge of controlling the DC bus voltage [10]. During this scenario, it is essential to be aware of the connection state of the DC bus voltage forming converter. This will enable a quick and spotless transition of the DC bus voltage control in case of failure. [9]. This has been strongly emphasized in [12], where a review of DC networks is shown, including its future challenges. [12] makes it clear that one of the main challenges of DC and hybrid DC/AC networks is related to islanding state detection, due to the absence of security standards and functionality.

The process of detecting the connection status of generators and loads to the main grid is known as islanding detection. A variety of methods have been proposed for DC microgrids [10], [13]–[21]. Two main categories are commonly used in the literature to group the methods according their characteristics:

- Active and passive methods: an active method [10], [17]–[20] requires to inject a disturbance to estimate the grid connection state. In contrast, passive methods [15], [16], [21] work as an observer. Both passive and active implementations can be found in practice:

TABLE 1. Comparison of methods for islanding detection in DC.

Technology	Description	Passive Active	Detection Time	Pros and Cons
Impedance Estimation	[13] Uses the incremental impedance calculated by a lock-in amplifier for islanding detection.	Active	16 ms	Pros: Easy to implement. Reliable. Cons: Not valid for multi-converter scenarios.
	[14] - Capacitor-based estimator using RLS.	Passive	10 ms	Pros: Fast and reliable in single-converter scenarios. Cons: Does not allow simultaneous detection in multi-converter scenarios.
	[15] - Calculates the cumulative sum of the output impedance.	Passive	80 ms	Pros: Reliable operation. Cons: Not valid for simultaneous islanding.
DC Voltage variation	[16] - Looks for variations in the DC-link voltage for DC islanding detection.	Passive	500 ms	Pros: Ease of use. Valid for multi-converter scenarios. Cons: Not reliable. Shows non detection zones.
	[17] - Tries to inject an AC component to the DC bus voltage to detect islanding.	Active	350 ms	Pros: Reliable in single-converter scenarios or with a low number of converters (less than 5). Cons: Not scalable for multi-converter scenarios since it needs a different frequency for each converter.
	[18] - Perturbs and observes the DC bus voltage by using current injection.	Active	200 ms	Pros: Easy to implement. Cons: disturbance can affect the PV operating point and reduce MPPT efficiency.

passive islanding techniques in DC look for unwanted voltage variations (or changes in the harmonic content of the DC bus voltage) while active methods try to perturb and observe the DC bus voltage. Passive techniques show non-detection zones, while active methods may cause rough variations within the DC voltage magnitude. Special care should be taken with multi-converter operation if an active method is implemented, because the injected disturbance may be cancelled by the other converters involved in the DC bus voltage control.

- Estimation technology: The detection of islanding in DC is more challenging than in AC since AC systems have more parameters to monitor: output impedance, magnitude, phase and frequency. Conversely, in DC these parameters are reduced to two: output impedance and voltage magnitude. Impedance detection techniques have been successfully used for islanding detection purposes in AC systems [22]–[28]. In DC systems, these methods are based on the output impedance estimation to detect changes in the grid connection state [13]–[15]. A second group of islanding DC techniques are based on the bus voltage monitoring [16]–[18]. The estimation of islanding relies on whether the bus voltage is operating within the nominal operating ranges.

The voltage monitoring techniques can be at the same time passive or active. They have been trendy in recent years [10], [16], [17], [19]–[21] and they are usually based on the Rate of Change of Voltage (ROCOV, passive implementation) [10] or on the Sandia Voltage Shift (SVS, active implementation) techniques. The main drawback of these techniques is that the positive-feedback islanding techniques deteriorate the stability of the system and may violate bus voltage controllability requirements. Regarding the voltage control of the DC bus, IEC 60038:2009 [29] specifies that LV systems can tolerate a steady-state voltage variation of $\pm 10\%$ at the supply voltage terminals. CENELEC EN 50160:2010 [30] for low voltage grids outlines a $\pm 10\%$ magnitude variation to be accomplished 95% of the time of the week. It allows 5% rapid voltage variations (normal), and 10% rapid voltage changes (infrequent). ANSI C84.1-2016 [31] states that voltage fluctuations should not normally exceed $\pm 5\%$ of the rated values. IEEE Standard 1159-2019 [32] does not take into account voltage changes within 10 percent of their nominal value. At the same time, IEEE Standard 1250-2018 [33] stipulates a voltage variation of $\pm 5\%$ in steady-state conditions. Therefore, the boundary of working conditions is a maximum variation of $\pm 5\%$ in the DC nominal voltage.

Another disadvantage of these methods is that no active voltage variation-based methods have been proposed that work in multi-converter scenarios. At the same time, passive methods show zones of non-detection, mainly if the demanded power is close to the generated.

Regarding the impedance detection methods in DC systems, their working principle has already been demonstrated in single-converter scenarios [13]–[15]. Later on in this work, it will be found out that they cannot directly be implemented with multi-converter microgrids due to the interactions among converters that result in a reduction of estimated impedance with parallel converters. In this situation, the converters act as a sink for the disturbance signal; the more converters are connected in parallel, the lower the estimated output impedance (see Fig. 1). This causes the difference between grid-connected and island impedance estimations to be very small, not detecting the island situation.

Therefore, the target application of the proposed technique is both purely DC microgrids or hybrid AC/DC microgrids or distribution systems, which would allow power to pass through multiple paths (DC or AC). The limits of power flow exchange between different devices (DC generators, energy storage, DC loads, single-phase and three-phase inverters) make it necessary to perform early and reliable islanding detection to ensure voltage control stability.

Table 1 summarizes the best performing methods in each of the categories described above. In summary, the

performance of passive methods is inadequate to ensure a high level of protection in DC microgrids. Active voltage variation methods can lead to potential instabilities in the DC bus voltage control and cannot be implemented in multi-converter scenarios. Impedance estimation-based methods provide high performance, but they cannot be directly applied to multi-converter scenarios.

This paper proposes a novel, distributed islanding detection method for DC muti-converter microgrids. The proposed method is based on the injection of a small AC pilot signal (frequency ω_p) and a Leader/Follower strategy that uses a pilot signal cancellation (PSC) scheme to allow multi-converter scenarios. The proposed method allows fast, accurate, and simultaneous detection of the grid-connection state (islanded or grid-connected) by all converters in the DC microgrid. Moreover, the proposed method does not require communications between the converters and its performance is independent of the microgrid topology.

To illustrate how the method works, Fig. 1 shows a sample DC microgrid using the proposed Leader/Follower islanding detection method; the AC/DC converter (Leader) injects the pilot signal and uses it to estimate the impedance and differentiate between islanded and grid connected modes. In the case of using a standard active impedance estimation strategy [13], [14], if other converters are added to the microgrid (for example, the dark color PV and storage converters), the resulting impedance will decrease and make the detection tough. In the proposed method, the follower converters implement a self synchronizing PSC scheme that results in a virtual disconnect at ω_p (faded PV and storage converters). This results in that, regardless of the number of converters connected to the DC microgrid, the impedance estimate seen from the Leader is not affected by the connection of the Followers. Simultaneously, by monitoring the injected component to implement the PSC, the followers detect the islanding condition without the need for communications.

The strongest contribution of the present work is to enable the implementation of active DC islanding detection methods based on impedance estimation in multi-converter scenarios. This issue, to the best knowledge of the authors, has not been previously addressed.

The paper is as organized as follows: Section II carries the theoretical analysis of the proposed technique, both for single and multi-converter scenarios. AC pilot signal parameter selection, stability and implementation concerns are developed in Section III, while the simulation evaluation of the method is performed in Section IV. Experimental tests of Section V validate the method.

II. ISLANDING DETECTION IN DC MICROGRIDS USING PILOT SIGNAL INJECTION & CANCELLATION

Figure 2 shows a diagram of a DC microgrid connected to the main grid. The DC microgrid includes a grid interface converter (red), which regulates the DC bus voltage (v_{bus}) in normal operation. Besides the grid interface converter, the microgrid includes other converters that interface with

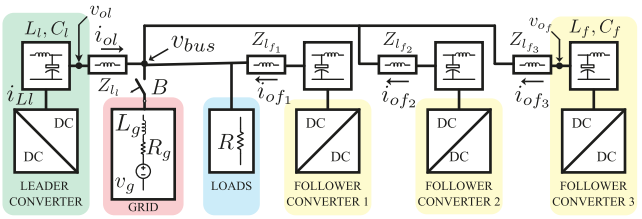

FIGURE 2. Topology of the DC microgrid under study. The model includes a set of power converters (Leader and Followers), the main grid model, loads, and line impedances between each of the converters and the point of common coupling. It also includes the converter LC filters and a connection breaker between the microgrid and the main grid. Finally, the measurement point is shown for all the electrical variables involved.

distributed generation assets (such PV or wind generators), energy storage systems, and other type of loads supplied by converters (single-phase inverters or DC-DC converters). The model also includes the impedance of the distribution lines (Z_l), and a resistance (R) that emulates the load demand.

The existence of active loads, such as Constant Power (CPL) or Constant Current (CCL), does not have a noticeable impact on the performance of the proposed method. This conclusion was deeply expanded in [13], where the effect of the line impedance and the bandwidth of the CPL controller and the line inductance are shown. [13] shows that, even with significant bandwidth reduction, mixture of loads, and line inductance, the islanding detection based on incremental impedance can be clearly differentiated. Because of this, and in order to simplify the theoretical analysis of the proposed method, a resistive load has been used as the equivalent of the power consumed in the DC bus.

Finally, the grid model includes a series resistance (R_g) that models a finite-power connection. The power converters in the microgrid are separated in leader (the one that injects the pilot current) and followers (which perform the PSC). If the grid interface converter looses the ability to regulate v_{bus} (islanding event), the other converters must detect this condition and switch to a different operating mode.

This section presents the proposed islanding detection method, built into the leader and follower converters. First, the section describes the operation of the leader converter, which is valid for a microgrid that only includes one additional converter as well as the case with multiple converters. Then, the algorithm of the follower converters is presented. This algorithm allows accurate, simultaneous, and independent detection in each converter without communications. This allows smooth transition between modes, allowing the DC microgrid to quickly form an independent island.

A. LEADER-CONVERTER OPERATION

For a single-converter operation, the proposed islanding detection technique is based on impedance detection through the injection of an AC pilot signal. The converter adds a sinusoidal signal ($i^*_{Lp_l}$, voltage or current, angular frequency ω_p) to its DC reference $i^*_{L_{DC_l}}$ (1)-(2) to estimate

the output impedance at that pilot frequency ($\vec{\hat{Z}}_o$). The pilot current signal injection has been selected in this work since it does not affect the DC transient behavior and it brings an improved control over the injected signal. Extended analysis of the voltage/current implementations can be found in Section III, where the pilot signal parameter selection and implementation concerns are also developed. The converter equivalent output impedance ($\vec{\hat{Z}}_o$) can be estimated through digital signal processing (3). To clarify the notation, if a generic signal x is used, x_p stands for the pilot frequency component of the x signal. It can be easily obtained using a band-pass filter (BPF) (4), its natural angular frequency being ω_p. Simultaneously, the $\vec{x}$ notation stands for a complex signal that can be obtained from x by using a Quadrature Signal Generator (QSG). This mechanism, which has been widely used for the single-phase synchronization task [34], generates a 90-degree component to its sinusoidal input. Many QSGs can be found in the literature [13], [35]–[41], the Second Order Generalized Integrator (SOGI) QSG is employed in this work due to its intrinsic filtering capability, smooth transient response, and ease of use.

$$i^*_{L_l} = i^*_{LDC_l} + i^*_{Lp_l} \tag{1}$$

$$i^*_{Lp_l} = I_{Lp_l} \cdot cos(\omega_p t) \tag{2}$$

$$\vec{\hat{Z}}_o = \frac{\vec{v}_{op_l}}{\vec{i}_{op_l}} \tag{3}$$

$$BPF(s) = \frac{2\zeta\omega_p s}{s^2 + 2\zeta\omega_p s + \omega_p^2} \tag{4}$$

$$\vec{\hat{i}}_{op_l} = \vec{i}_{Lp_l} - j\vec{v}_{op_l}\omega_p C_l \tag{5}$$

The proposed technique does not require any additional measurement since the converter output voltage (v_{ol}) and current (i_{ol}) are usually measured to implement droop-control strategies [42]. If i_o is not measured, it can be estimated by using the inductor current (i_L), the output voltage (v_o), and the filter capacitance value (C_l, Fig. 4). In the case that a faithful capacitance measurement is not available, one of the estimation methods defined in the literature can be used [43].

Therefore, in a single-converter scenario, the $\vec{\hat{Z}}_o$ output impedance (3) is used as an estimator for islanding detection, the single converter being called Leader. In grid-connected mode, $\vec{\hat{Z}}_o$ tends to the parallel connection of the load and the grid impedances (R and R_g in Fig. 2). Since it is expected that R_g to be much lower than R (and close to zero), $\vec{\hat{Z}}_o \rightarrow R_g \rightarrow 0$. Conversely, in island mode, there is only a load (or set of loads) connected to the converter's output. In this case, it is clear that $\vec{\hat{Z}}_o \rightarrow R$.

Fig. 3a shows the Leader converter impedance estimator. Details of the implementation of the SOGI can be found in [37]. Note that K sets the SOGI bandwidth, $K = \sqrt{2}$ is usually set to provide the best transient response [44].

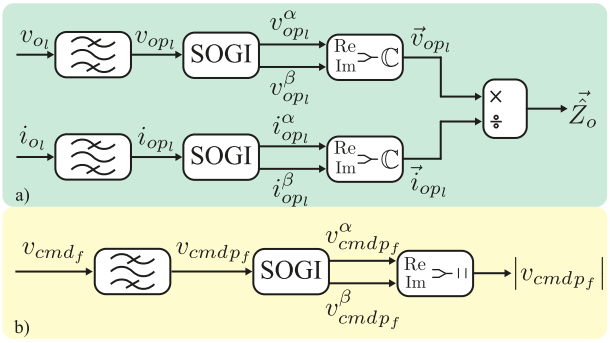

FIGURE 3. a) Leader and b) Follower converter block diagrams for islanding detection. In the Leader case, the output impedance estimate ($\vec{\hat{Z}}_o$) is used as the figure of merit for islanding detection. In contrast, the Followers use the magnitude of the compensation voltage command ($|v_{cmd_f}|$).

B. MULTICONVERTER OPERATION

DC Microgrids establish a multi-converter scenario. Generation (PV, Wind), storage (flywheels, batteries, supercaps), and even loads (inverters, lighting, EV chargers, telecommunication) are connected to the DC bus by using DC-DC converters. If more than one converter is connected in parallel, (Figs. 1 and 2), and each of them were to use the strategy introduced in Section II-A, there would be obstacles to providing a suitable performance:

1) Unwanted interactions will occur among converters if they all inject the pilot signal at the same ω_p. In this case, even if the injection is performed synchronized to avoid circulating currents [45], the converter output impedance estimation (3) cannot be used for islanding detection purposes since each converter injects a portion of the total pilot current.
2) A possible solution to the previous problem could be using a different ω_p for each converter. This is not a scalable solution in general, while v_{bus} and load/grid currents will be highly distorted.
3) Parallel converters consume pilot current if only one converter injects the pilot signal (see Figs. 1 and 2). This is because each converter is controlling its inductor current (i_L) to follow a DC reference, the pilot current being absorbed by the converter capacitor (see Fig. 4, red color). This results in a reduction of $\vec{\hat{Z}}_o$ (3), causing the accuracy of the method to depend on the network topology and the number of parallel converters. At the same time, the remaining converters cannot detect the islanding situation.

Thus, the AC pilot injection with impedance detection purposes is not reliable in multi-converter scenarios. A Leader/Follower approach is proposed in this section to generalize its use in multi-converter scenarios. While the Leader implements the algorithm in Section II-A, the followers implement an independent and complementary strategy. One converter will be defined as *Leader*, injecting the AC pilot signal, all other converters working as *Followers*.

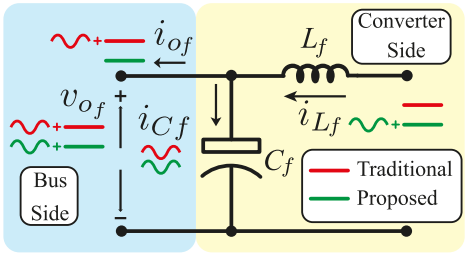

FIGURE 4. Detail of the follower converter voltage and currents for the traditional and the proposed AC pilot signal cancellation (PSC). In the traditional case (red color), the Follower converter output current (i_{of}) includes both a DC and an AC components due to the Leader AC injection. In the proposed method (green color) the Follower converter injects the AC current from the converter side (i_{Lf}). This causes the AC current on the output side of the filter to be zero. This results in a virtual disconnection of the Follower converter from the DC bus at the pilot frequency (ω_p).

Converters with grid-forming capabilities are candidates as Leaders while the rest of converters work as Followers.

To prevent Followers from absorbing the pilot signal injected by the Leader, they will work in a *high-impedance* mode at ω_p (see Fig. 4, green color). Thus, they will be *virtually disconnected* from the bus at ω_p. To do so, since the follower's capacitor C_f absorbs pilot current (i_{Cpf}) (the DC bus voltage is slightly polluted by the Leader), what is proposed here is to provide i_{Cpf} from the converter-side, i_{Lpf}, making the output current (i_{opf}) zero. This allows the Leader to use the same impedance detection technique as in the single-converter scenario (see Section II-A and Fig. 3a), its island state being determined upon the output impedance estimation. Followers will use their pilot voltage command for islanding detection. The pilot bus voltage will tend to zero in grid-connected state since the DC grid sets a stiff DC bus voltage. Conversely, in island mode, v_{bus} will be slightly distorted by the Leader at ω_p, each Follower requiring a non-zero pilot voltage command to work in infinite-impedance mode. Fig. 3b shows the Follower block diagram for islanding detection. It uses the same SOGI and BPF blocks as the Leader, as shown in Fig. 3a. Note that v_{cmd_f} is the Follower current controller action, extended details being found in Section III.

III. PILOT SIGNAL PARAMETER SELECTION AND IMPLEMENTATION CONCERNS

A. PILOT SIGNAL INJECTION TECHNIQUES

The Leader converter may use two pilot signal injection methods: voltage or current-based, their implementations being shown in Fig. 5a and b. In the voltage-based injection technique, Fig. 5a, the pilot signal is added as a duty-cycle disturbance to the proportional-integral (PI) controller command [27], [28], the injected current not being controlled. This requires to filter out the current measurement (or the controller input) to prevent the current controller to react to the injected signal. This may lead to instability conditions (or transient deterioration) depending on ω_p, the current controller's bandwidth, and the notch filters. On the other hand, the current-based injection implementation (Fig. 5b)

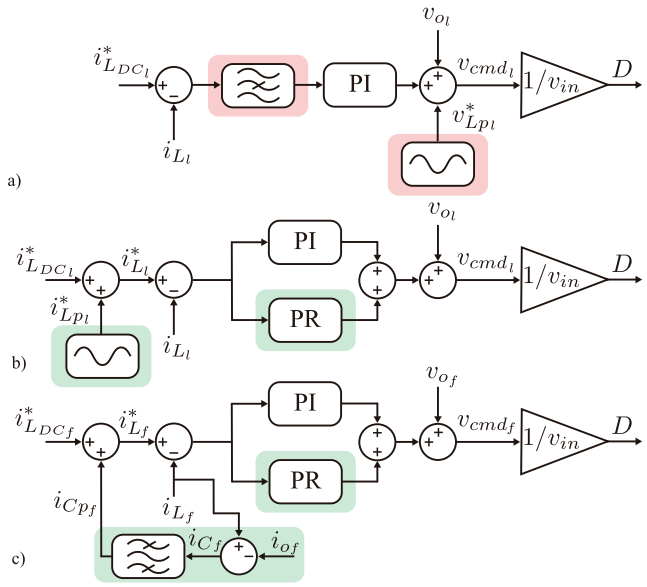

FIGURE 5. a) Voltage and b) Current pilot signal injection block diagrams (Leader Converter). c) Pilot signal cancellation (PSC) block diagram. (Follower converter.)

adds the pilot signal as a reference to the current control loop. This requires implementing a proportional-resonant (PR) controller, the DC behavior of the converter being not degraded. Fig. 5c shows the Follower converter current control block diagram including the PSC. This implementation is independent of the Leader signal injection technique and is based on a current control implemented by a parallel PI-PR structure. This control structure is well known and provides an excellent performance. At the same time, it does not affect to the stability of the system [46]–[51]. A pilot current signal injection is used in this work since it does not affect the DC transient behavior, and it brings an improved control over the injected signal. Simultaneously, having the same current control structure in all converters allows quickly changing the converter's role if necessary.

B. PILOT SIGNAL PARAMETER SELECTION

The Leader converter should select the magnitude and frequency of the pilot signal to disturb v_{bus} as little as possible. At the same time, it should allow accurate detection of the grid-connection state. The following constraints have been considered:

1) Pilot signal frequency (ω_p): Each DC-DC converter feeds an output capacitor for filtering purposes (C_l). Thus, the converter output current (i_{ol} in Fig. 2) depends on both the capacitor's value and the equivalent output impedance. Thus, the current divisor rule can be applied to obtain the $H_d = i_{ol}(s)/i_{Ll}(s)$ transfer function (6), where $Z_{eq}(s)$ refers to the equivalent impedance of the entire circuit (capacitor in parallel with output impedance) and $Z_o(s)$ refers to the output impedance.

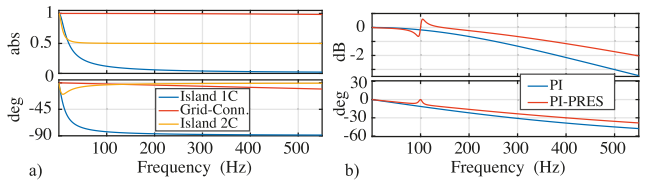

FIGURE 6. Frequency analysis. a) H_d (6) Bode plot for different grid connection states. b) Closed-loop current control for PI and PI-PR structures. 1C refers to 1 converter operation while 2C stands for 2 converters operating in parallel.

Fig. 6a shows the Bode plot of H_d for three configurations: single-converter feeding a load (R) in island mode (Fig. 6a blue (7)), single-converter feeding a load in grid-connected mode (Fig. 6a orange (8), where R_g and L_g are the grid resistance and inductance respectively) and two converters (Fig. 2 with capacitors C_l and C_f) connected in parallel feeding a load in island mode (Fig. 6a yellow (9)).

It can be noted that the worst case occurs when a single converter feeds a resistive load in island mode. In this situation, the higher ω_p, the lower i_o. In grid-connected mode, most the injected current is absorbed by the grid due to its lower impedance. Finally, if two converters are connected in parallel, the pilot current is distributed among the converters' capacitors.

$$H_d = \frac{i_{ol}(s)}{i_{Ll}(s)} = \frac{Z_{eq}(s)}{Z_o(s)} \tag{6}$$

$$H_{d1C} = \frac{1}{C_l R s + 1} \tag{7}$$

$$H_{dGC} = \frac{L_g s + R_g + R}{C_l L_g R s^2 + (L_g + C_l R_g R)s + R_g + R} \tag{8}$$

$$G_{d2C} = \frac{C_f R s + 1}{(C_l + C_f)R s + 1} \tag{9}$$

For the particular case of the setup that follows Fig. 2 and Table 2, a frequency of 100 Hz is selected to provide fast detection (higher frequencies allow to increase the detection speed), have enough spectral separation between the DC and the pilot components and to reduce the current absorbed by the capacitor in island mode.

2) Pilot signal magnitude: The pilot signal should be as low as possible since it disturbs v_{bus} in island mode and i_g in grid-connected mode. The minimum pilot signal amplitude is limited by the sensitivity of the available sensors and resolution of the analog-to-digital conversion (ADC) stages. Pilot signal amplitudes ranging from 0.5% to 1% are realizable using industry-standard sensing and ADC stages.
3) Bandwidth of the Leader/Follower current control: Since the pilot signal is injected in current, the current control bandwidth must ensure that it is properly injected. Fig. 6b shows the closed-loop bode plot for the leader converter following Fig. 2 and Table 2 for PI and PI-PR control structures. If a PI control strategy is used, the closed-loop phase delay (11.3 degrees at 100 Hz) does not allow to inject the pilot signal component properly. This effect occurs even under high control bandwidth (500 Hz). This is critical for the Follower converter case since this control bandwidth would not allow to fully compensate its output current, which would affect the impedance estimation on the Leader converter.
4) Double-frequency ripple in single-phase rectifiers: The use of single-phase AC-DC converters induces a double line frequency ripple (100 or 120 Hz) in the DC bus current and voltage [52], [53]. This frequency should be avoided for this application to elude undesired interactions.

TABLE 2. Setup parameters.

Symbol	Parameter	Value
R	Bus load	50 Ω
f_s	Switching frequency	10 kHz
L_l	Leader filter inductance	2 mH
L_f	Followers filter inductance	2.2 mH
C_l, C_f	Leader & Follower filter capacitance	270 μF
Z_{l_l}	Leader Distribution Line Impedance	0.5 Ω, 0.05 mH
$Z_{l_{f_1}}$	Follower 1 Distribution Line Impedance	1 Ω, 0.1 mH
$Z_{l_{f_2}}$	Follower 2 Distribution Line Impedance	1.5 Ω, 0.15 mH
$Z_{l_{f_3}}$	Follower 3 Distribution Line Impedance	2 Ω, 0.2 mH
R_g	Grid resistance	0.2 Ω
BW_{PI}	PI bandwidth	500 Hz
BW_{PR}	PR bandwidth	50 Hz
ω_p	Pilot frequency	2π 100 Hz
I_{Lp}	Pilot magnitude	0.3 A

In conclusion, a 0.3 A, 100 Hz pilot signal (a 60 Hz three-phase AC-DC converter is assumed) will be injected by the Leader converter, which satisfies all of the above restrictions. Simultaneously, both Leader and Follower converters will use a PI-PR control structure, its parameters being shown in Table 2.

C. STABILITY ANALYSIS

As illustrated in Fig. 5, a traditional output voltage feed-forward term is employed to cancel the second order dynamics in the current control loop. Following a conservative control design approach that highlights the low dynamic requirements of the proposed method, the bandwidth of the current loop PI controller is set one decade below the Nyquist frequency, at 500Hz. The PI controller gains are tuned following conventional methods to cancel the pole given by the series resistance and inductance ratio and to obtain the desired current control bandwidth. As shown in the block diagrams in Fig. 5b and c, the PR controller adds to the PI branch. As illustrated in Fig. 7a, the PR controller bandwidth is set one decade below the PI bandwidth, at 50Hz, to limit the

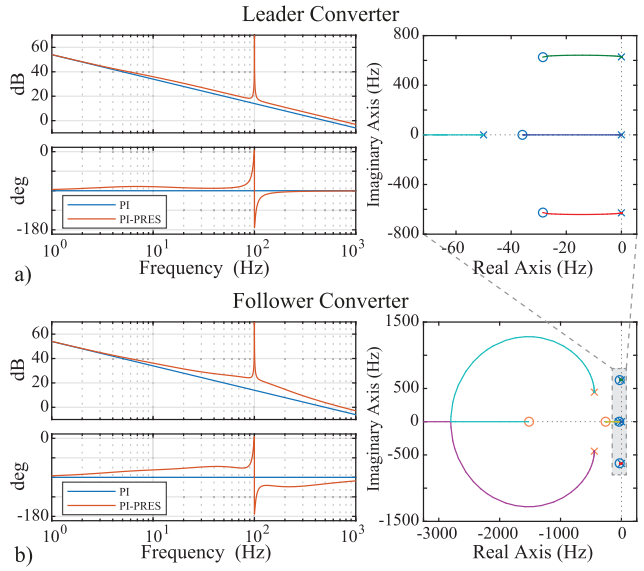

FIGURE 7. a) Leader and b) Follower converters open-loop transfer function and root locus.

effects of this branch to the pilot signal frequency (100Hz) and minimize the dynamic effects at all other frequencies.

In the leader converter, the pilot signal is injected by adding to the desired DC current $i^*_{L_{DC_l}}$. The stability can then be ensured by analyzing the open-loop transfer function or the location of the roots. As shown in Fig. 7a, a 90° phase margin is obtained.

In the follower converter, the pilot signal cancellation generates additional considerations for the stability analysis. As illustrated in Fig. 5c the follower converter inductor current feedback path is given by: $1 + BPF(s)$. Then, the follower converter stability can be ensured by employing the open-loop transfer function and root locus shown in Fig. 7b. As detailed in these graphs, the additional feedback path mostly affects the low frequency behaviour, resulting in a phase margin of 78°.

IV. SIMULATION EVALUATION

The initial evaluation of the proposed method is performed using PLECS simulations. To test the performance of the method, the setups shown in Fig. 2 and Fig. 8 were used for the multiconverter and leader only tests respectively. The test parameters are found in Table 2.

A. LEADER-CONVERTER OPERATION

The model used for the Leader-converter operation is shown in Fig. 8. It includes the Leader converter, the main grid model, loads, and line impedance between the Leader converter and the point of common coupling. It also includes the converter LC filter and a connection breaker between the microgrid and the main grid. Fig. 9a shows the breaker B connection status. The converter starts isolated from the grid, and a grid connection is performed at t=0.5s. The converter is returned to island operation at t=1.5s. Fig. 9b shows the converter output current (i_{ol} in Fig. 2). The converter injects

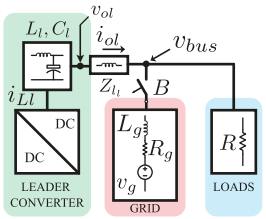

FIGURE 8. Leader-converter evaluation setup. The model includes the Leader converter, the main grid model, loads, and line impedance between the Leader converter and the point of common coupling. It also includes the converter LC filter and a connection breaker between the microgrid and the main grid.

the necessary amount of current to maintain the DC bus voltage to 375V, including at the same time the pilot signal component. As predicted by Fig. 6a, the output pilot current component changes from island to grid-connected operation, leading to a small disturbance (1V, $\approx$ 0.002 p.u.) in the DC bus voltage in island operation (Fig. 9c). The injection of the pilot wave results in an ripple of the DC bus voltage of 0.56% in islanded mode. In grid-connected mode, the DC-bus pilot voltage component is zero due to the low grid impedance. Its finally shown in Fig. 9d the absolute value of the output impedance estimation (3), including a couple of insets to verify its transient behavior. The bus load is accurately estimated in island operation (50 Ω), while a near-zero impedance is estimated in grid connection state. Thus, the proposed technique shows an excellent response detecting the islanding situation (detection takes less than 15 *ms*.). For islanding detection, the IEEE Std 1547-2018 [54] states that, for an unintentional island in which the distributed energy resource (DER) energizes a portion of the electric power system (EPS) area through the PCC, the DER shall detect the island, cease to energize the Area EPS, and trip within 2s of the formation of an island. The proposed method is 133 times faster than suggested by the standards. The detection is, in this case, fast and reliable since the existence of no detection zones (NDZ) is not considered. At the same time, IEEE Standard 2030.7-2017 [55] states that microgrids are capable to operate in the islanding mode and supply local loads, but also connected to the grid at the point of interconnection. In this regard, the standard indicates that distributed generation systems must be able to detect islanding conditions, but does not indicate the maximum islanding detection time.

B. MULTICONVERTER OPERATION

Results for the multi-converter scenario are shown in Fig. 10, where the same test procedure as in Fig. 9 was performed. In this case, the Leader and three Follower converters share the DC load current, as shown in Fig. 10b. It is clear from that figure that the Leader injects the pilot signal while the Followers work in high-impedance mode (there is no pilot current component in their output currents). The v_{bus} (Fig. 10c) remains unchanged from the previous experiment in this case (0.6% deviation), which indicates that the proposed PSC is working correctly. Figs. 10d and Fig. 10e show the Leader

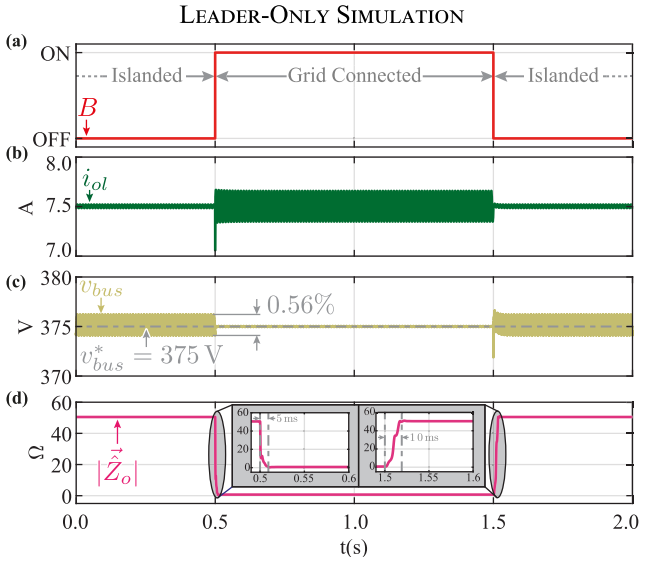

FIGURE 9. Simulation evaluation for Leader-converter operation: a) breaker status (*B*) that transitions the DC microgrid between states, Breaker OFF means that the microgrid is disconnected from the main grid., b) converter output current (i_{ol}), c) bus voltage (v_{bus}), and d) estimated converter output impedance ($|\hat{Z}_o|$). The insets show the $|\hat{Z}_o|$ during the change between islanded and connected to the main grid; the detection takes less that 10ms.

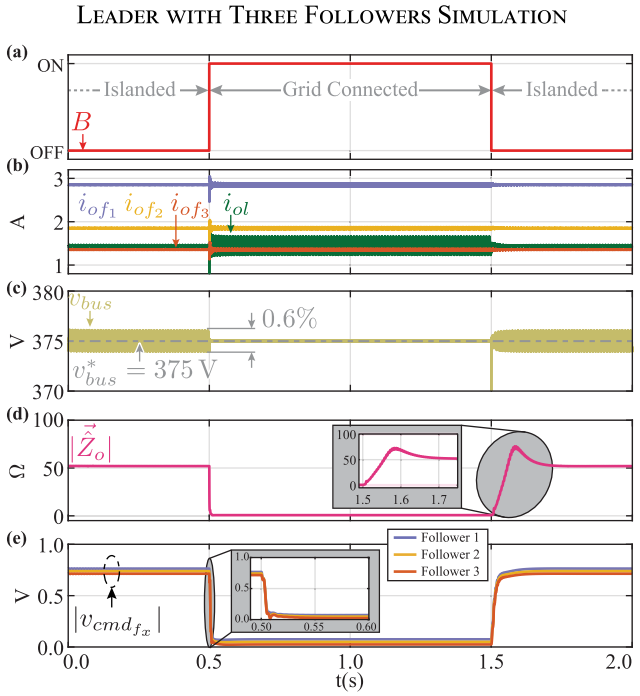

FIGURE 10. Simulation evaluation for multi-converter operation with one leader converter and three follower converters: a) breaker status (*B*) that transitions the DC microgrid between states, b) converter output currents (i_{ol}, i_{of_n}), c) bus voltage (v_{bus}), d) estimated Leader output impedance ($|\hat{Z}_o|$), and e) Pilot signal commands ($|\hat{v}_{cmdp_{f_x}}|$) of each follower converter. The insets show the $|\hat{Z}_o|$ of the leader and $|\hat{v}_{cmdp_{f_x}}|$ of each follower during the change between islanded and connected to the main grid; the detection takes less that 15ms.

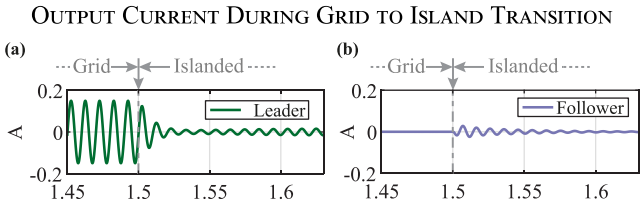

FIGURE 11. Simulation evaluation: grid disconnection effect on the pilot signal injected by the leader(a) and its effect in the follower (b).

and Followers islanding detection estimators (the estimated impedance and the pilot cancellation signal). It must be noted that fast, accurate, and simultaneous detection is achieved without communication between the converters. The Follower converters are *virtually disconnected* at ω_p, and therefore they do not affect the Leader's impedance estimation.

For the particular case of the islanding event, (t=1.5s) there is a different transient response than the one obtained in the single-converter operation of Fig. 9, This effect does not provide any false detection and does not affect the method's speed. This is shown in Fig. 11 for better understanding, where the pilot current of the Leader and Follower converters are shown around the islanding event. Since the leader converter's output pilot current is not controlled (only the inductance current i_{Ll} its controlled), the non-ideal cancellation given by a limited transient response at the Followers affects the Leader estimation. A higher current-loop gain at the pilot signal frequency should be set to limit this effect, which is not possible in this work due to the closeness of the filter resonant frequency. It only affects the transient estimation of the bus resistance.

To test the immunity of the proposed method to load changes on the DC bus, a load change test has been performed both in island and in grid-connected conditions. The results of this test are shown in Fig. 12, where the value of the load connected to the DC bus is shown in Fig. 12d. The remaining signals shown in Fig. 12 are the same as in the previous test shown in Fig. 10. The microgrid starts working at the nominal voltage of the main grid (375V), in islanded condition. As in the previous experiment, both the Leader and the set of Followers accurately detect the island condition. The Leader detects an impedance of 50Ω (Fig. 12e), while the set of Followers present pilot cancellation signals different from 0 (Fig. 12f). At t=0.25s the DC bus load (*R* in Fig. 2) is changed by 20%. As can be seen in Fig. 12, the Leader and Followers islanding detection estimators (the estimated impedance of Fig. 12e and the pilot cancellation signals of Fig. 12f) are minimally affected by the load change. The Leader correctly detects the load variation, while the Followers are practically unaffected in their pilot cancellation voltages.

At t=1.25s, when the DC microgrid is grid-connected, the DC-bus load is returned to 50Ω (Fig. 12d). As shown in Fig. 12e and Fig. 12f, the behavior of the proposed method under load variations is outstanding. Leader and Follower estimates are almost unaffected by DC-bus load changes. It can be concluded from this test that variations in the

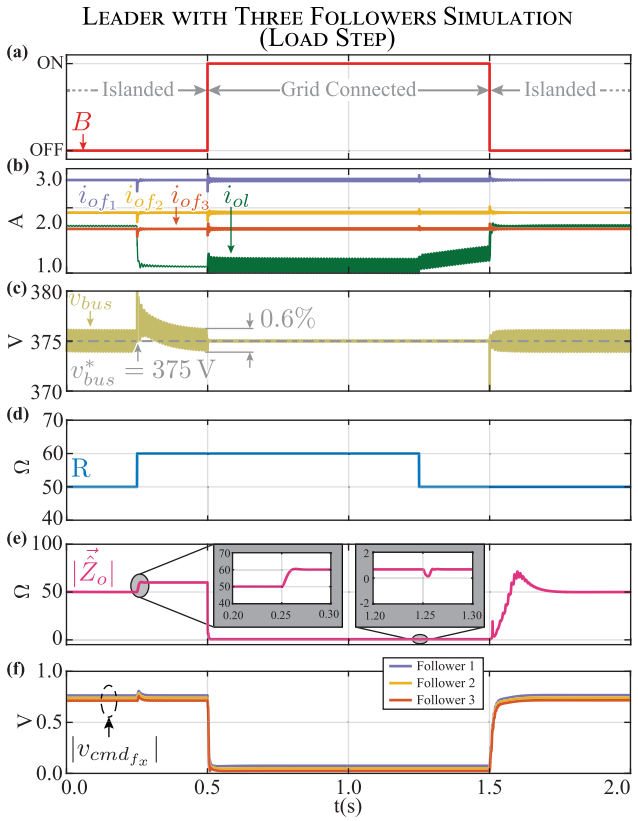

FIGURE 12. Simulation evaluation for multi-converter operation with one leader converter and three follower converters. Response to a load-step: a) breaker status (*B*) that transitions the DC microgrid between states, b) converter output currents (i_{ol}, i_{of_n}), c) bus voltage (v_{bus}), d) DC-bus load *R*,e) estimated Leader output impedance ($|\hat{Z}_o|$), and f) Pilot signal commands ($|\hat{v}_{cmdp_{f_x}}|$) of each follower converter. The insets show the $|\hat{Z}_o|$ of the leader and $|\hat{v}_{cmdp_{f_x}}|$ of each follower during the change between islanded and connected to the main grid when the DC-bus load is modified. The method shows an outstanding performance, being practically unaffected by DC-bus load changes.

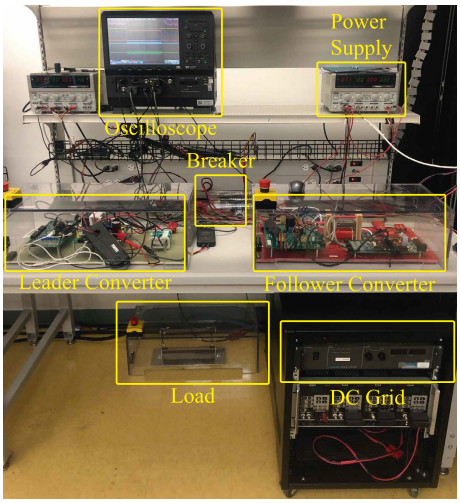

FIGURE 13. Photo for the experimental Setup. Center-left and right-hand sides show the Leader and Follower converters, including the grid breaker. Bottom left and right-hand sides show the resistive load and grid respectively. The top of the photo shows the auxiliary power supplies and the oscilloscope.

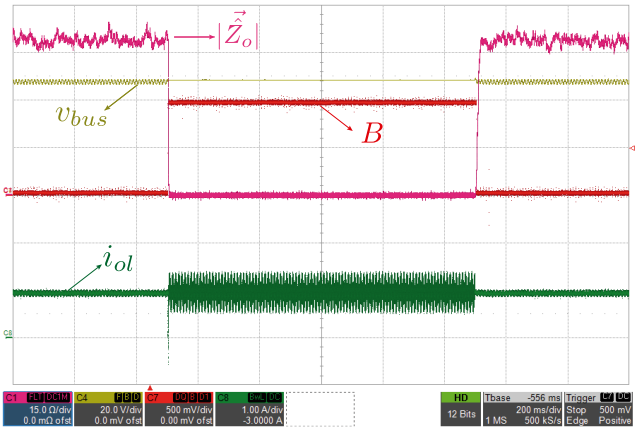

FIGURE 14. Experimental results: Leader-converter operation. Breaker status (red), converter output current (i_{ol} green), bus voltage (v_{bus} brown), estimated Leader output impedance ($|\hat{Z}_o|$ pink).

DC bus load do not adversely affect the sensitivity and reliability of the proposed method.

V. EXPERIMENTAL VERIFICATION

Experimental verification has been carried out by using the laboratory-scale setup shown in Fig. 13. A couple of parallel DC-DC converters switching at 10 kHz were used to feed a 50Ω load; the whole microgrid is connected to the main grid by means of a DC breaker. The DC-DC converters are controlled by using Texas Instruments F28335 DSPs. As in Section IV, both single and multi-converter scenarios are considered. The following figures will show both electrical measurements (bus voltage, converter currents…) and internal variables from both DSPs (estimated impedance and voltage command absolute value), represented as voltages by using digital to analog converters.

A. LEADER-CONVERTER OPERATION

Experimental results for the Leader-converter scenario are shown in Fig. 14. As in the simulation test, the setup follows Fig. 8. The same colors as in the simulations were used for more straightforward presentation, while similar grid connection/disconnection events were performed. Simulation (Fig. 9) and experimental (Fig. 14) results show excellent agreement. The voltage in island mode (brown color) contains the pilot signal component, while it disappears when the converter is grid-connected. The single converter estimates its output equivalent impedance (pink color) with high accuracy (50Ω in island, ≈ 0Ω in grid-connected mode). Simultaneously, the estimation speed matches the one obtained in simulation (15 ms). Therefore, the output impedance estimation is an appealing solution for islanding detection in single-converter scenrios.

B. MULTICONVERTER OPERATION

Figure 15 shows the experimental verification of the proposed method in a multi-converter scenario. These results are in

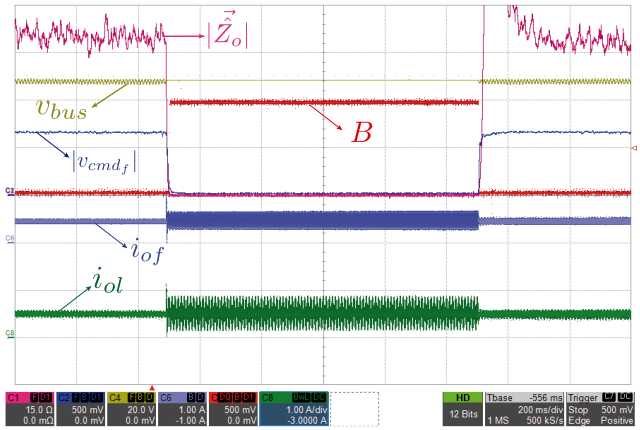

FIGURE 15. Experimental results: multi-converter operation with one leader converter and a follower converter: Breaker status (red), converter output currents (i_{ol} green, i_{of} purple), bus voltage (v_{bus} brown), estimated Leader output impedance ($|\hat{Z}_o|$ pink), and Follower pilot signal command ($|\hat{v}_{cmdp_f}|$ blue).

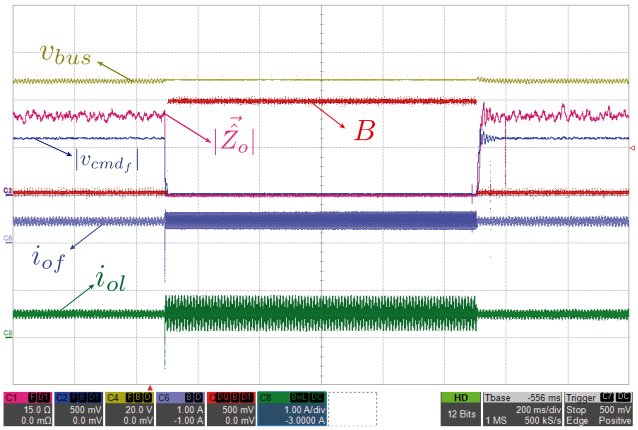

FIGURE 16. Experimental results: multi-converter operation. Follower converter includes only a PI controller with a bandwidth of 500 Hz. Breaker status (red), converter output currents (i_{ol} green, i_{of} purple), bus voltage (v_{bus} brown), estimated Leader output impedance ($|\hat{Z}_o|$ pink), and Follower pilot signal command ($|\hat{v}_{cmdp_f}|$ blue).

good agreement with the simulations (Fig. 10). The Follower converter works in high-impedance mode, its pilot voltage command shown in blue color. Note that it can be used for islanding detection purposes, since it offers a value of 0.75V and 0V in island and grid-connected modes, respectively. Simultaneously, the Leader output impedance estimation (pink) does not vary from the single-converter scenario. The presence (Leader, green) and absence (Follower, purple) of the pilot signal component in the converter output currents are finally noted.

The previous set of experimental tests have been validated the performance of the proposed technique. A group of extended results has been included to test the performance of the method under non-ideal conditions. First, Fig. 16 shows the estimation results when the Follower converter does not include a PR controller in its current control (Fig. 5); a PI controller is used with a bandwidth of 500 Hz. As analyzed in Section III-B, although the PI bandwidth is high compared to ω_p, the Follower converter is not able to fully compensate its input pilot current (purple color) due to the closed-loop delay shown in Fig. 6b. This reduces the Lead converter output impedance estimation (pink color) to 28 Ω. The Follower converter can still detect the islanding situation, although it reduces the Follower pilot command variation between island and grid-connected mode (blue color). This effect increases the smaller the PI bandwidth.

Its finally shown in Fig. 17 the effect of having a non-zero grid impedance (R_g in Fig. 2). In this test, a 1.5 Ω resistance is used to emulate a finite-power grid. While in island mode, the Leader and Follower estimations are the same as in Fig. 15 (the grid impedance does not have any influence), in grid-connected mode v_{bus} (brown color) is slightly polluted by the Leader pilot injection. Thus, the Leader output impedance estimation in grid-connected mode rounds 1.5 Ω (the method accurately estimates the output impedance). The Follower converter is able to detect the islanding event by looking to its compensation voltage.

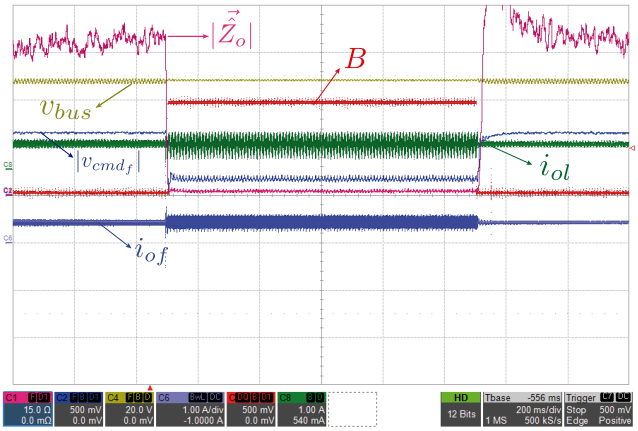

FIGURE 17. Experimental results: multi-converter operation. Follower converter includes both PI and PR Controllers. Finite Power Grid with a series resistance of 1.5 Ω. Breaker status (red), converter output currents (i_{ol} green, i_{of} purple), bus voltage (v_{bus} brown), estimated Leader output impedance ($|\hat{Z}_o|$ pink), and Follower pilot signal command ($|\hat{v}_{cmdp_f}|$ blue).

This experiment allows to show that, in a real case, the pilot component of follower compensation is not exactly zero. This is an interesting result, since it makes it possible to detect the absence of the Leader and to implement a strategy for reassigning the Leader role. If the Leader converter is intentionally or unintentionally disconnected from the grid, some strategies (involving communications or not) can be used to reassign the Leader-role. This reassignment problem has been solved in practice in AC systems in the past [28] and can be solved in the same way in DC. Followers can detect the absence of the Leader by monitoring the magnitude of the compensation signal. As soon as the absence of the Leader is detected, the competitive strategy described in [28] can be implemented.

VI. CONCLUSION

This paper proposed an islanding detection technique for single and multi-source DC microgrids based on the AC pilot

injection. A theoretical analysis was performed, while the control and parameter selection guidelines were also defined. The proposed method allows simultaneous and independent islanding detection of each converter connected to the DC bus since it follows a Leader/Follower strategy. The method was validated by detailed theoretical analysis, as well as simulation and experimental tests. From the obtained results, it can be concluded the high reliability, fast detection, and smooth transient response of the method, while its accuracy is independent of the microgrid topology.

REFERENCES

[1] P. Yang, Y. Xia, M. Yu, W. Wei, and Y. Peng, "A decentralized coordination control method for parallel bidirectional power converters in a hybrid AC–DC microgrid," *IEEE Trans. Ind. Electron.*, vol. 65, no. 8, pp. 6217–6228, Aug. 2018, doi: 10.1109/TIE.2017.2786200.

[2] P. Wang, C. Jin, D. Zhu, Y. Tang, P. C. Loh, and F. H. Choo, "Distributed control for autonomous operation of a three-port AC/DC/DS hybrid microgrid," *IEEE Trans. Ind. Electron.*, vol. 62, no. 2, pp. 1279–1290, Feb. 2015, doi: 10.1109/TIE.2014.2347913.

[3] A. Ballo, A. D. Grasso, G. Palumbo, and T. Tanzawa, "Charge pumps for ultra-low-power applications: Analysis, design, and new solutions," *IEEE Trans. Circuits Syst. II, Exp. Briefs*, vol. 68, no. 8, pp. 2895–2901, Aug. 2021, doi: 10.1109/TCSII.2021.3070889.

[4] M. Forouzesh, P. Y. Siwakoti, A. S. Gorji, F. Blaabjerg, and B. Lehman, "Step-up DC–DC converters: A comprehensive review of voltage-boosting techniques, topologies, and applications," *IEEE Trans. Power Electron.*, vol. 32, no. 12, pp. 9143–9178, Dec. 2017, doi: 10.1109/TPEL.2017.2652318.

[5] B. Axelrod, Y. Berkovich, and A. Ioinovici, "Switched-capacitor/switched-inductor structures for getting transformerless hybrid DC–DC PWM converters," in *Proc. IEEE Int. Symp. Circuits Syst. (ISCAS)*, Mar. 2008, vol. 55, no. 2, pp. 687–696, doi: 10.1109/TCSI.2008.916403.

[6] W. Li and X. He, "Review of nonisolated high-step-up DC/DC converters in photovoltaic grid-connected applications," *IEEE Trans. Ind. Electron.*, vol. 58, no. 4, pp. 1239–1250, Apr. 2011, doi: 10.1109/TIE.2010.2049715.

[7] B. Zhao, S. Qiang, W. Liu, and Y. Sun, "Overview of dual-active-bridge isolated bidirectional DC–DC converter for high-frequency-link power-conversion system," *IEEE Trans. Power Electron.*, vol. 29, no. 8, pp. 4091–4106, Aug. 2014, doi: 10.1109/TPEL.2013.2289913.

[8] A. Chub, D. Vinnikov, F. Blaabjerg, and F. Z. Peng, "A review of galvanically isolated impedance-source DC–DC converters," *IEEE Trans. Power Electron.*, vol. 31, no. 4, pp. 2808–2828, Apr. 2016, doi: 10.1109/TPEL.2015.2453128.

[9] L. Meng, Q. Shafiee, G. F. Trecate, H. Karimi, D. Fulwani, X. Lu, and J. M. Guerrero, "Review on control of DC microgrids and multiple microgrid clusters," *IEEE J. Emerg. Sel. Topics Power Electron.*, vol. 5, no. 3, pp. 928–948, Sep. 2017, doi: 10.1109/JESTPE.2017.2690219.

[10] A. M. I. Mohamad and Y. A.-R.-I. Mohamed, "Assessment and performance comparison of positive feedback islanding detection methods in DC distribution systems," *IEEE Trans. Power Electron.*, vol. 32, no. 8, pp. 6577–6594, Aug. 2017, doi: 10.1109/TPEL.2016.2618220.

[11] G. Villa, S. Saeed, P. Garcia, C. Gomez-Aleixandre, and R. Georgious, "Compensation alternatives for power sharing mismatch in multiport DC–DC–AC converters," *IEEE Trans. Ind. Appl.*, vol. 57, no. 6, pp. 6221–6236, Nov. 2021, doi: 10.1109/TIA.2021.3115721.

[12] S. Augustine, J. Quiroz, M. J. Reno, and S. Brahma, "DC microgrid protection: Review and challenges," U.S. Dept. Energy Office Sci. Tech. Inf., Oak Ridge, TN, USA, Aug. 2018. [Online]. Available: https://www.osti.gov/biblio/1465634, doi: 10.2172/1465634.

[13] F. Paz and M. Ordonez, "An impedance-based islanding detection method for DC grids," in *Proc. 9th IEEE Int. Symp. Power Electron. Distrib. Gener. Syst. (PEDG)*, Jun. 2018, pp. 1–7, doi: 10.1109/PEDG.2018.8447714.

[14] C. Blanco, P. Garcia, A. Suarez, and I. Pelaez, "Impedance estimator for multi-source DC microgrids with islanding detection capabilities," in *Proc. IEEE Energy Convers. Congr. Expo. (ECCE)*, Oct. 2020, pp. 1325–1329, doi: 10.1109/ECCE44975.2020.9235366.

[15] B. K. Choudhury and P. Jena, "Superimposed impedance-based passive islanding detection scheme for DC microgrids," *IEEE J. Emerg. Sel. Topics Power Electron.*, vol. 10, no. 1, pp. 469–483, Feb. 2021, doi: 10.1109/JESTPE.2021.3076459.

[16] F. Ghalavand, I. Al-Omari, H. K. Karegar, and H. Karimipour, "Hybrid islanding detection for AC/DC network using DC-link voltage," in *Proc. IEEE Int. Conf. Smart Energy Grid Eng. (SEGE)*, Aug. 2018, pp. 216–221.

[17] Q. Huang, H. Chen, X. Xiang, C. Li, W. Li, and X. He, "Islanding detection with positive feedback of selected frequency for DC microgrid systems," *IEEE Trans. Power Electron.*, vol. 36, no. 10, pp. 11800–11817, Oct. 2021, doi: 10.1109/TPEL.2021.3066486.

[18] G. S. Seo, K. C. Lee, and B. H. Cho, "A new DC anti-islanding technique of electrolytic capacitor-less photovoltaic interface in DC distribution systems," *IEEE Trans. Power Electron.*, vol. 28, no. 4, pp. 1632–1641, Apr. 2013, doi: 10.1109/TPEL.2012.2208226.

[19] S. Dhar and P. K. Dash, "Performance analysis of a new fast negative sequence power injection oriented islanding detection technique for photovoltaic photovoltaic based voltage source converter based micro grid operation," *IET Gener., Transmiss. Distrib.*, vol. 9, no. 15, pp. 2079–2090, Nov. 2015, doi: 10.1049/iet-gtd.2015.0369.

[20] A. M. I. Mohamad and Y. A.-R. I. Mohamed, "Analysis and mitigation of interaction dynamics in active DC distribution systems with positive feedback islanding detection schemes," *IEEE Trans. Power Electron.*, vol. 33, no. 3, pp. 2751–2773, Mar. 2018, doi: 10.1109/TPEL.2017.2699233.

[21] C. N. Papadimitriou, V. A. Kleftakis, and N. D. Hatziargyriou, "A novel method for islanding detection in DC networks," *IEEE Trans. Sustain. Energy*, vol. 8, no. 1, pp. 441–448, Jan. 2017, doi: 10.1109/TSTE.2016.2604419.

[22] D.-U. Kim and S. Kim, "Anti-islanding detection method using phase-shifted feed-forward voltage in grid-connected inverter," *IEEE Access*, vol. 7, pp. 147179–147190, 2019, doi: 10.1109/ACCESS.2019.2946317.

[23] O. P. Mahela, Y. Sharma, S. Ali, B. Khan, and S. Padmanaban, "Estimation of islanding events in utility distribution grid with renewable energy using current variations and stockwell transform," *IEEE Access*, vol. 9, pp. 69798–69813, 2021, doi: 10.1109/ACCESS.2021.3078315.

[24] N. K. Swarnkar, O. P. Mahela, B. Khan, and M. Lalwani, "Identification of islanding events in utility grid with renewable energy penetration using current based passive method," *IEEE Access*, vol. 9, pp. 93781–93794, 2021, doi: 10.1109/ACCESS.2021.3092971.

[25] F. S. Al-Ismail, "DC microgrid planning, operation, and control: A comprehensive review," *IEEE Access*, vol. 9, pp. 36154–36172, 2021, doi: 10.1109/ACCESS.2021.3062840.

[26] S. K. G. Manikonda and D. N. Gaonkar, "Comprehensive review of IDMs in DG systems," *IET Smart Grid*, vol. 2, no. 1, pp. 11–24, Mar. 2019, doi: 10.1049/iet-stg.2018.0096.

[27] D. Reigosa, F. Briz, C. B. Charro, P. Garcia, and J. M. Guerrero, "Active islanding detection using high-frequency signal injection," *IEEE Trans. Ind. Appl.*, vol. 48, no. 5, pp. 1588–1597, Sep. 2012, doi: 10.1109/TIA.2012.2209190.

[28] D. Reigosa, F. Briz, C. Blanco, P. García, and J. M. Guerrero, "Active islanding detection for multiple parallel-connected inverter-based distributed generators using high-frequency signal injection," *IEEE Trans. Power Electron.*, vol. 29, no. 3, pp. 1192–1199, Mar. 2014, doi: 10.1109/TPEL.2013.2263845.

[29] *IEC Standard Voltages*, Standard IEC 60038:2009, 2009.

[30] *Voltage Characteristics of Electricity Supplied by Public Electricity Networks*, Standard CENELEC EN 50160, 2010.

[31] *American National Standard for Electric Power Systems and Equipment—Voltage Ratings (60 Hz)*," Standard ANSI C84.1, 2016.

[32] *IEEE Recommended Practice for Monitoring Electric Power Quality*, IEEE Standard 1159-2019 (Revision IEEE Std 1159-2009), 2019, pp. 1–98, doi: 10.1109/IEEESTD.2019.8796486.

[33] *IEEE Guide for Identifying and Improving Voltage Quality in Power Systems*, IEEE Standard 1250-2018 (Revision IEEE Std 1250-2011), 2018, pp. 1–63, doi: 10.1109/IEEESTD.2018.8532376.

[34] S. Golestan, J. M. Guerrero, and J. C. Vasquez, "Single-phase PLLs: A review of recent advances," *IEEE Trans. Power Electron.*, vol. 32, no. 12, pp. 9013–9030, Dec. 2017, doi: 10.1109/TPEL.2017.2653861.

[35] S. Golestan, J. M. Guerrero, A. Vidal, A. G. Yepes, J. Doval-Gandoy, and F. D. Freijedo, "Small-signal modeling, stability analysis and design optimization of single-phase delay-based PLLs," *IEEE Trans. Power Electron.*, vol. 31, no. 5, pp. 3517–3527, May 2016, doi: 10.1109/TPEL.2015.2462082.

[36] S. Golestan, M. Monfared, F. D. Freijedo, and J. M. Guerrero, "Dynamics assessment of advanced single-phase PLL structures," *IEEE Trans. Ind. Electron.*, vol. 60, no. 6, pp. 2167–2177, Jun. 2013, doi: 10.1109/TIE.2012.2193863.

[37] M. Ciobotaru, R. Teodorescu, and F. Blaabjerg, "A new single-phase PLL structure based on second order generalized integrator," in *Proc. 37th IEEE Power Electron. Spec. Conf. (PESC)*, Jun. 2006, pp. 1–6, doi: 10.1109/pesc.2006.1711988.
[38] C. Blanco, D. Reigosa, F. Briz, and J. M. Guerrero, "Quadrature signal generator based on all-pass filter for single-phase synchronization," in *Proc. Energy Convers. Congr. Expo. (ECCE)*, Sep. 2014, pp. 2655–2662, doi: 10.1109/ECCE.2014.6953757.
[39] I. Galkin and M. Vorobyov, "Optimizing of sampling in a low-cost single-phase instantaneous AC-grid synchronization unit with discrete calculation of derivative function," in *Proc. IECON 41st Annu. Conf. IEEE Ind. Electron. Soc.*, Nov. 2015, pp. 004538–004543, doi: 10.1109/IECON.2015.7392807.
[40] X. Fang, Y. Wang, M. Li, and J. Liu, "A novel frequency-adaptive PLL for single-phase grid-connected converters," in *Proc. IEEE Energy Convers. Congr. Expo.*, Sep. 2010, pp. 414–419, doi: 10.1109/ECCE.2010.5618000.
[41] P. Hao, W. Zanji, and C. Jianye, "A measuring method of the single-phase AC frequency, phase, and reactive power based on the Hilbert filtering," *IEEE Trans. Instrum. Meas.*, vol. 56, no. 3, pp. 918–923, Jun. 2007.
[42] G. Liu, T. Caldognetto, P. Mattavelli, and P. Magnone, "Power-based droop control in DC microgrids enabling seamless disconnection from upstream grids," *IEEE Trans. Power Electron.*, vol. 34, no. 3, pp. 2039–2051, Mar. 2019, doi: 10.1109/TPEL.2018.2839667.
[43] H. Soliman, H. Wang, and F. Blaabjerg, "A review of the condition monitoring of capacitors in power electronic converters," *IEEE Trans. Ind. Appl.*, vol. 52, no. 6, pp. 4976–4989, Nov. 2016, doi: 10.1109/TIA.2016.2591906.
[44] P. Rodríguez, A. Luna, R. S. Muñoz-Aguilar, I. Etxeberria-Otadui, R. Teodorescu, and F. Blaabjerg, "A stationary reference frame grid synchronization system for three-phase grid-connected power converters under adverse grid conditions," *IEEE Trans. Power Electron.*, vol. 27, no. 1, pp. 99–112, Jan. 2012, doi: 10.1109/TPEL.2011.2159242.
[45] C. Blanco, D. Reigosa, J. C. Vasquez, J. M. Guerrero, and F. Briz, "Virtual admittance loop for voltage harmonic compensation in microgrids," *IEEE Trans. Ind. Appl.*, vol. 52, no. 4, pp. 3348–3356, Jul. 2016, doi: 10.1109/TIA.2016.2547362.
[46] M. Liserre, R. Teodorescu, and F. Blaabjerg, "Multiple harmonics control for three-phase grid converter systems with the use of PI-RES current controller in a rotating frame," *IEEE Trans. Power Electron.*, vol. 21, no. 3, pp. 836–841, May 2006, doi: 10.1109/TPEL.2006.875566.
[47] J. Hu, Y. He, L. Xu, and B. W. Williams, "Improved control of DFIG systems during network unbalance using PI–R current regulators," *IEEE Trans. Ind. Electron.*, vol. 56, no. 2, pp. 439–451, Feb. 2009, doi: 10.1109/TIE.2008.2006952.
[48] L. Herman, I. Papic, and B. Blazic, "A proportional-resonant current controller for selective harmonic compensation in a hybrid active power filter," *IEEE Trans. Power Del.*, vol. 29, no. 5, pp. 2055–2065, Oct. 2014, doi: 10.1109/TPWRD.2014.2344770.
[49] A. Kulkarni and V. John, "Mitigation of lower order harmonics in a grid-connected single-phase PV inverter," *IEEE Trans. Power Electron.*, vol. 28, no. 11, pp. 5024–5037, Nov. 2013, doi: 10.1109/TPEL.2013.2238557.
[50] A. Hasanzadeh, O. C. Onar, H. Mokhtari, and A. Khaligh, "A proportional-resonant controller-based wireless control strategy with a reduced number of sensors for parallel-operated UPSs," *IEEE Trans. Power Del.*, vol. 25, no. 1, pp. 468–478, Jan. 2010, doi: 10.1109/TPWRD.2009.2034911.
[51] M. F. Iacchetti, G. D. Marques, and R. Perini, "Torque ripple reduction in a DFIG-DC system by resonant current controllers," *IEEE Trans. Power Electron.*, vol. 30, no. 8, pp. 4244–4254, Aug. 2015, doi: 10.1109/TPEL.2014.2360211.
[52] K. Mozaffari, M. Amirabadi, and Y. Deshpande, "A single-phase inverter/rectifier topology with suppressed double-frequency ripple," *IEEE Trans. Power Electron.*, vol. 33, no. 11, pp. 9282–9295, Nov. 2018, doi: 10.1109/TPEL.2018.2797125.
[53] Y. Qiu, L. Wang, H. Wang, Y.-F. Liu, and P. C. Sen, "Bipolar ripple cancellation method to achieve single-stage electrolytic-capacitor-less high-power LED driver," *IEEE J. Emerg. Sel. Topics Power Electron.*, vol. 3, no. 3, pp. 698–713, Sep. 2015, doi: 10.1109/JESTPE.2015.2433918.
[54] *IEEE Standard for Interconnection and Interoperability of Distributed Energy Resources With Associated Electric Power Systems Interfaces*, IEEE Standard 1547-2018 (Revision IEEE Std 1547-2003), 2018, pp. 1–138, doi: 10.1109/IEEESTD.2018.8332112.
[55] *IEEE Standard for the Specification of Microgrid Controllers*, IEEE Standard 2030.7-2017, 2018, pp. 1–43, doi: 10.1109/IEEESTD.2018.8340204.

CRISTIAN BLANCO (Member, IEEE) was born in Villablino, Leon, Spain. He received the B.S. degree in telecommunications engineering and the M.S. and Ph.D. degrees in electrical engineering from the University of Oviedo, Gijon, Spain, in 2010, 2011, and 2015, respectively.

From September 2012 to February 2013, he was a Ph.D. Guest at Aalborg University, Denmark. From July 2019 to December 2019, he was a Visiting Faculty at The University of British Columbia, Canada. He is currently an Associate Professor with the Department of Electrical, Computer, and Systems Engineering, University of Oviedo. He is also works with the LEMUR Research Team. In 2011, he was awarded a fellowship of the Personnel Research Training Program funded by the Regional Ministry of Education and Science of the Principality of Asturias. His research interests include modeling and control of islanded and grid-connected converters including storage systems, synchronization, islanding detection and power quality, microgrids, and digital signal processing. He was the recipient of an IEEE Energy Conversion Congress and Exposition Second Prize Paper Award, in 2013, and the University of Oviedo Outstanding Ph.D. Thesis Award, in 2016.

FRANCISCO PAZ (Member, IEEE) was born in La Plata, Argentina. He received the degree in electronics engineering from the National University of Comahue, Neuquén, Argentina, in 2012, and the M.A.Sc. and Ph.D. degrees in electrical engineering from The University of British Columbia (UBC), Vancouver, BC, Canada, in 2014 and 2020, respectively.

He was a Lecturer for several courses on renewable energy systems and electronics under the Vancouver Summer Program, from 2016 to 2019, and delivered tutorials at IEEE SPEC 2017, IEEE PEDG 2018/2019, and IEEE ECCE 2018/2020. He is currently a Research Associate at UBC, where he works on power electronics for renewable energy sources, energy storage, and DC microgrids. His industrial experience includes work for EnerSys/Alpha Technologies, Burnaby, BC, Canada, where he worked on the development of remote DC power systems for 5G.

Dr. Paz received several scholarships and awards, including the prestigious Killam Graduate Teaching Assistant Award, in 2018, and the Best Conference Paper awarded by PELS Technical Committee 5 (TC5) at PEDG.

IGNACIO GALIANO ZURBRIGGEN (Member, IEEE) was born in San Francisco, Cordoba, Argentina. He received the Ing. degree in electronics engineering from the National University of Cordoba, Argentina, in 2010, and the M.A.Sc. and Ph.D. degrees from The University of British Columbia (UBC), Canada, in 2013 and 2020, respectively.

His work in power electronics includes industrial research and development experience at COMPUTROL Ingenieria Electronica, San Francisco, designing and implementing power conversion platforms and digital controllers. His current research interests include the study of linear, non-linear, and mixed control strategies for power electronic converters applied to renewable energy systems, electric vehicles, battery chargers, and microgrids.

Dr. Zurbriggen has delivered multiple technical presentations and seminars, and he also serves as a reviewer for several IEEE/IET/Wiley journals and conferences.

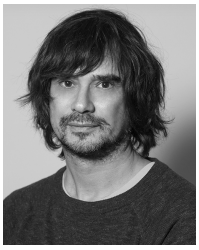

PABLO GARCIA (Senior Member, IEEE) received the M.S. and Ph.D. degrees in electrical engineering and control from the University of Oviedo, Gijon, Spain, in 2001 and 2006, respectively. In 2004, he was a Visitor Scholar with the Wisconsin Electric Machines and Power Electronics Consortium, University of Madison–Wisconsin, Madison, WI, USA. He is currently an Associate Professor with the Department of Electrical, Computer, and Systems Engineering, University of Oviedo. Regarding his teaching activities, he is the Co-Coordinator of the Erasmus Mundus Master Course in ''Sustainable Transportation and Electrical Power Systems''—STEPS (http://www.emmcsteps.eu). During many years he worked in alternating-current (ac) drives, sensorless control, ac machines diagnostics, magnetic bearings, and signal processing. Nowadays he is focused on power converters working as a connection interface of renewable energy and storage systems to the electrical grid. He was a recipient of the 2005 IEEE TRANSACTIONS ON INDUSTRY APPLICATIONS, Third Place Prize Paper Award, and two IEEE Industry Applications Society Conference prize paper awards, in 2006 and 2010, respectively.

MARTIN ORDONEZ (Member, IEEE) was born in Neuquen, Argentina. He received the Ing. degree in electronics engineering from the National Technological University, Cordoba, Argentina, in 2003, and the M.Eng. and Ph.D. degrees in electrical engineering from the Memorial University of Newfoundland (MUN), St. John's, NL, Canada, in 2006 and 2009, respectively.

He was an Adjunct Professor with Simon Fraser University, Burnaby, BC, Canada, and MUN. He is currently a Professor and the Canada Research Chair of power converters for renewable energy systems with the Department of Electrical and Computer Engineering, The University of British Columbia, Vancouver, BC, Canada. He is also the holder of the Fred Kaiser Professorship on Power Conversion and Sustainability at UBC. His industrial experience in power conversion includes research and development at Xantrex Technology Inc./Elgar Electronics Corporation (currently AMETEK Programmable Power, San Diego, CA, USA). With the support of industrial funds and the Natural Sciences and Engineering Research Council, he has contributed to more than 150 publications and R&D reports.

Dr. Ordonez was the recipient of the David Dunsiger Award for Excellence in the Faculty of Engineering and Applied Science, in 2009, and the Chancellors Graduate Award/Birks Graduate Medal, in 2006, and he became a fellow of the School of Graduate Studies, MUN.